RSC Advances

ROYAL SOCIETY OF CHEMISTRY

www.rsc.org/advances

Cite this: DOI: 10.1039/c0xx00000x

www.rsc.org/xxxxxx

ARTICLE TYPE

One-pot synthesis of a TiO_2-CdS nano-heterostructure assembly with enhanced photocatalytic activity

Sayantan Mazumdar[a] and Aninda J. Bhattacharyya*[a]

Received (in XXX, XXX) Xth XXXXXXXXX 20XX, Accepted Xth XXXXXXXXX 20XX

DOI: 10.1039/b000000x

An unprecedented morphology of titanium dioxide (TiO_2) and cadmium sulfide (CdS) self-assembly obtained using a 'truly' one-pot and highly cost effective method with a multi-gram scale yield is reported here. The TiO_2–CdS assembly, comprising of TiO_2 and CdS nanoparticles residing next to each other homogeneously self-assembling into 'woollen knitting ball' like microspheres, exhibited remarkable potential as a visible light photocatalysts with high recyclability.

For quite some time now, development of novel functional materials has been primarily driven due to their constant demand in renewable energy and sustainable environment.[1] Design of materials via ambient or near ambient temperature synthesis methods for various applications is at the forefront of research interest worldwide.[2] Light induced degradation of chemical pollutants found in air and water to environmentally benign products is absolutely essential for sustainable development.[1b, 1c] Titania has been widely demonstrated as a photocatalyst for degradation of various pollutants owing to its favourable electronic properties, excellent chemical stability and cost effectiveness.[3] However, absorption in titania is limited to only the ultra-violet (UV) region of the solar spectrum due to its wide band gap (≈ 3.2 eV). This restricts its ability to absorb only 4-5% of the sunlight, thus making it an inefficient solar photon harvester.[1b, 1c, 4] As a result of these limitations related to pristine TiO_2, serious efforts are being made to widen the absorption spectrum of wide band gap materials such as TiO_2 and widen the scope of their applications. Doping of TiO_2 e.g. with a transition metal[5] or non-metal,[6] attachment of another metal nano structure[7] or metal oxide[8] to TiO_2 have achieved limited success in light induced degradation of chemical pollutants. Efficient light induced catalysis by materials constituting of noble metals as one of the key component have been demonstrated in recent times.[1b, 2e, 7, 9] However, usage of noble metals is expected to increase the cost of mass scale production by leaps and bounds.

Sensitization of titanium dioxide by another light harvesting semiconductor of lower band gap (around ~ 2 eV) is a very effective approach and has assumed great relevance in several photochemical applications.[10] Among various low band gap (≈ 2 eV) semiconductors, cadmium sulphide (II-VI semiconductor) has proven to be one of the most viable candidates owing to its unique electronic band structure. [11] The position of its conduction band edge is higher than that of titanium dioxide (even in the bulk) and as a result, favourable electron injection rates from the CdS to TiO_2 on ultrafast timescale can be achieved.[12] CdS also facilitates ease of synthesis due to its higher stability and yield compared to the other competitors like CdSe or CdTe. The effective electronic properties of the assembly of the wide and narrow band gap semiconductor can be additionally tuned by tailoring their geometry and spatial configuration at the nanoscale.[1h, 10c, 12] Attachment of the light harvester to the wide band gap semiconductor is also observed to be a key issue, as this, along with nanostructuring greatly affects the electron transfer kinetics and hence photochemical property of the semiconductor assembly.[12] Thus, the abundance and low cost of a TiO_2-CdS assembly with efficient electron transfer properties will be in great demand not only for the much discussed third generation photovoltaics but also for photocatalysis for spectral range wider than UV-regime. Approaches have been devised towards facile synthesis of TiO_2-CdS heterostructures for visible light photocatalysis and other related applications. In few cases, the synthesis involved multiple steps and the photocatalytic ability is not satisfactory. [2g-2j] Zhao *et al* reported a TiO_2-CdS heterostructure via a one-step solvothermal method with enhanced photocatalytic activity. [2i] However, the stability and reusability of the photocatalyst, which is a very vital issue for a photocatalyst for practical applications, was not reported.

In this work, a TiO_2-CdS nano-heterostructured assembly has been synthesized using a very facile and 'truly' one-pot synthesis method. The synthesis method yielded products in multi-gram scale quantity which is the necessary desired goal for any practical and industrial mass scale applications. The often much highlighted issue of toxicity associated with cadmium is easily tackled here by the remarkable stability and recyclability of the TiO_2-CdS assembly.

In a typical synthesis, a CdS precursor (e.g. L-cysteine as the S-precursor, c/f Experimental Section) along with a surfactant, (acting as the structure directing agent) are taken in a teflon container in a water-ethanol mixture. TiO_2-precursor is then added to the CdS-precursor-water-ethanol mixture and hydrolysed using acid. Solvent is evaporated by constant stirring. Subsequently, di-methyl formamide is added to the CdS precursor-surfactant-TiO_2-precursor mixture which was then subjected to a solvothermal reaction (c/f Experimental Section). The orange-yellow product is centrifuged, washed with water and ethanol and then dried in vacuum under mild heating condition.

Cite this: DOI: 10.1039/c0xx00000x

www.rsc.org/xxxxxx

ARTICLE TYPE

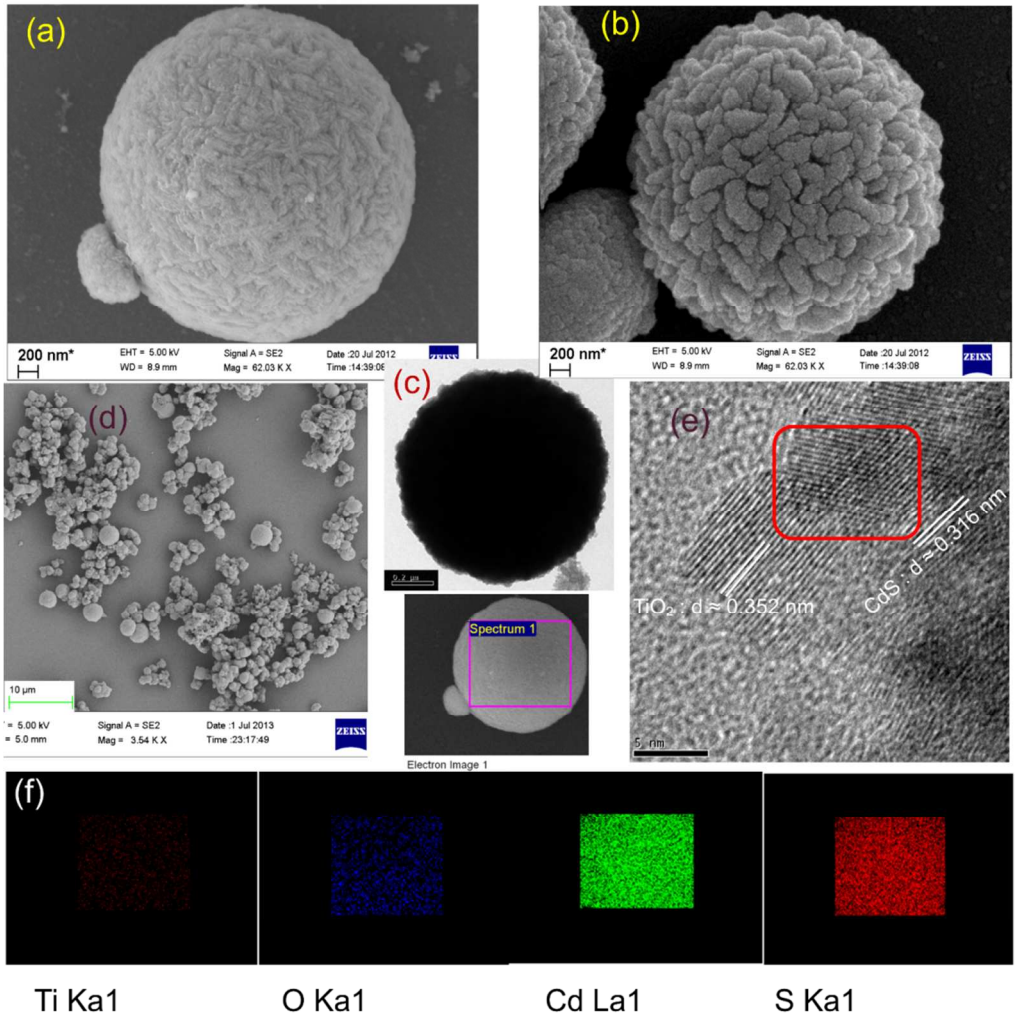

Figure 1. (a) and (b) Scanning electron microscope (SEM) images (at low accelerating voltage = 5 kV and slow scanning speed) of two representative 'woolen knitting ball' like microspheres, (c) low-resolution transmission electron microscope (TEM) images of a microsphere (scale = 200 nm), (d) low magnification SEM image, (e) representative high resolution transmission electron microscope (HRTEM) image of a small area of the microsphere showing an anatase TiO_2 nanoparticle [$d \approx 0.352$ nm (101) plane] and a wurtzite CdS nanoparticle [d ≈ 0.316 nm (101) plane]; Moiré pattern formed due to overlap of anatase TiO_2 (101) plane and wurtzite CdS (101) plane marked by red rounded rectangle (f) Elemental maps obtained by EDS of the same microsphere as in (a) on a rectangular area as marked in pink.

The dried product is subjected to further experimental investigations. Systematic investigations using scanning electron microscopy vividly reveal as synthesized products constituting of micrometre sized spheres (diameter ≈ 1 µm). These microspheres were in turn composed of nanometre sized particles of TiO_2 and CdS. Two of the representative SEM images are shown in figure 1 (a) and (b). The microspheres are observed to be ~1-2 µm in diameter and mimic a 'woolen knitting ball'. Identical types of 'woolen knitting balls' are found at various scanned areas of the sample along with few aggregates and smaller size spheres (c/f figure 1 (d) and S1). HRTEM on various parts of a single sphere and repeated on various microspheres reveal that anatase TiO_2 and mixed-phase CdS nanoparticles of very small size (~ 5 nm) reside very close to each other in a side by side configuration over the entire microsphere. For TiO_2 and CdS, the (101) plane is clearly visible. This is exactly identified by the interplanar spacing for anatase TiO_2 ($d_{101} \approx 0.352$ nm) and wurtzite CdS ($d_{101} \approx 0.316$ nm). The residence of TiO_2 and CdS nanoparticles next to each other can be seen very clearly in figure 1 (e) and figure S1. The observation of side by side residence of TiO_2 and CdS is also supported by elemental mapping of microspheres done via energy-dispersive X-ray spectroscopy (EDS) done on the same

microsphere as shown in figure 1 (a). The EDS shows a homogeneous distribution of all the constituent elements viz. Ti, O, Cd and S throughout the microsphere as demonstrated by the elemental mapping in figure 1 (f). Both the constituents i.e. TiO_2 and CdS showed high crystallinity at the nanometer scale as evidenced by the clear visibility of the planes in the HRTEM images. In few cases, (101) planes from anatase TiO_2 and wurtzite CdS are overlapped to form Moiré patterns which confirm good crystallinity as well as homogeneous distribution of both TiO_2 and CdS in all directions (c/f figure 1 (e) and figure S1). TiO_2 nanoparticles are formed under solvothermal conditions in an acidic medium and their growth is restricted by the surfactant (CTAB) present in the reaction mixture. CdS nanoparticles form due to reaction of Cd^{2+} and S^{2-} precursors during the solvothermal reaction in presence of the high boling point DMF solvent. Simultaneous formation of TiO_2 and CdS nanoparticles leads to a micro-sized spherical assembly where both of them reside next to each other. Presence of water and ethanol has a effect on the "woolen-knitting ball" like morphology. When the same reaction is carried out in the presence of DMF (i.e. in the absence of water and ethanol), microspheres formed but it does not resemble a "woolen knitting ball" like morphology. The surface characteristics appeared to be different (c/f figure S2) comapred to as shown in figure 1 (a, b).

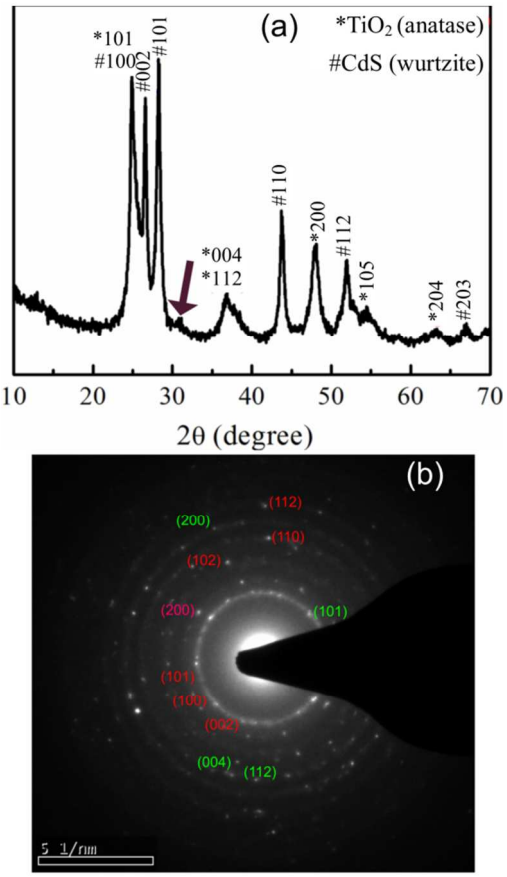

Figure 2. (a) Powder XRD pattern showing anatase TiO_2 (*) and wurtzite CdS (#); a small peak for zinc blende (200) plane at $2\theta = 30.7^0$ is also shown by an arrow (b) SAED pattern obtained from transmission electron microscope showing various planes for anatase TiO_2 (green), wurtzite CdS (red) and zinc blende CdS (pink).

The crystalline nature of the TiO_2-CdS assembly is also visible in the powder XRD pattern in figure 2 (a) where all the peaks are indexed to either anatase TiO_2 (JCPDS 21-1272) or predominantly to wurtzite CdS (JCPDS 41-1049). The mixed-phase nature of CdS is evidenced via the observation of a small peak at $2\theta=30.7^0$ (indicated by an arrow in figure 2 (a)) assigned to the zinc blende CdS (200) phase (JCPDS 80-0019). It is worth mentioning that the zinc blende (200) is the only significant peak for the zinc blende CdS which doesn't overlap with any of the wurtzite CdS peaks. The mixed phase nature of CdS is also evidenced from the SAED pattern shown in figure 2(b). Presence of kinetically favourable zinc blende phase is generally expected as the reaction has been carried out in a mixed solvent media solvothermally at low temperature.[10c, 13] The BET surface area of the TiO_2-CdS sample is found to be 66 m^2g^{-1} (c/f figure S3). Interestingly, the BJH pore distribution (c/f figure S4) reveals a microporous morphology (distribution maximum < 2 nm) for the TiO_2-CdS assembly.

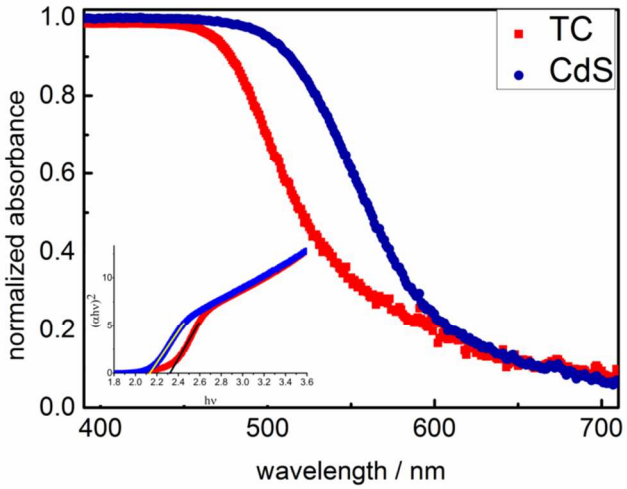

Figure 3. Absorbance spectra of TiO_2-CdS microsphere assembly (TC) and wurzite CdS, the Kubelka-Munk plots to measure the direct band gap are in inset.

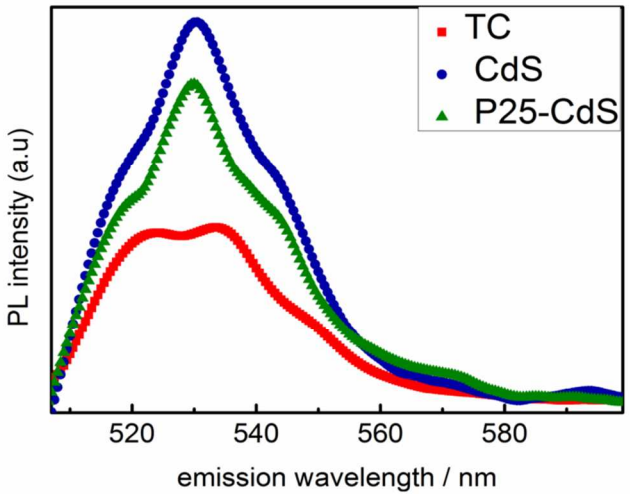

Figure 4. Photoluminescence spectra of TiO_2-CdS microsphere assembly (TC), wurzite CdS, wurtzite CdS:P25-TiO_2 mixture.

Steady state optical property is studied via absorbance and photoluminescence spectroscopy for the as synthesized TiO_2-CdS assembly, a wurtzite CdS sample and an equimolar mixture of the same wurtzite sample with commercially available Degussa P25–TiO_2. The wurtzite CdS sample, P25–TiO_2 and an equimolar mixture of P25-TiO_2:CdS were used as the benchmark materials to compare the properties with the as synthesized TiO_2-CdS assembly. Both of the samples exhibit onsets at similar wavelengths, the wurtzite CdS sample has a slightly broader absorption spectrum than the TiO_2-CdS assembly (c/f figure 3). The optical band gap estimated from the Kubelka-Munk plots are 2.32 eV and 2.15 eV for TiO_2-CdS assembly and CdS respectively. The P25-CdS sample absorption spectrum matches exactly with the wurtzite CdS sample. The band gap of the TiO_2-CdS assembly is smaller than that of bulk CdS value (= 2.42 eV), which is not unexpected in mixed-phase CdS nanomaterials.[10c]

Photoluminescence behaviour of the samples is also measured. In general, all the three samples exhibited broad emission characteristics however, the profiles were distinctly different for the TiO_2-CdS assembly compared to the other two samples (figure 4). The P25-CdS sample displayed a PL spectrum similar to the CdS but with lesser intensity compared to the CdS sample. This attributed to the transfer of electrons from conduction band of CdS to the conduction band of TiO_2. The TiO_2-CdS assembly displayed much lower intensity in the PL spectrum than the P25-TiO_2:CdS sample. Higher quenching of PL in the nano-heterostructured TiO_2-CdS assembly suggests a more favourable kinetics for electron transfer from the conduction band of CdS to the conduction band of TiO_2 compared to the physical mixture of CdS and P25-TiO_2.[1h 14]

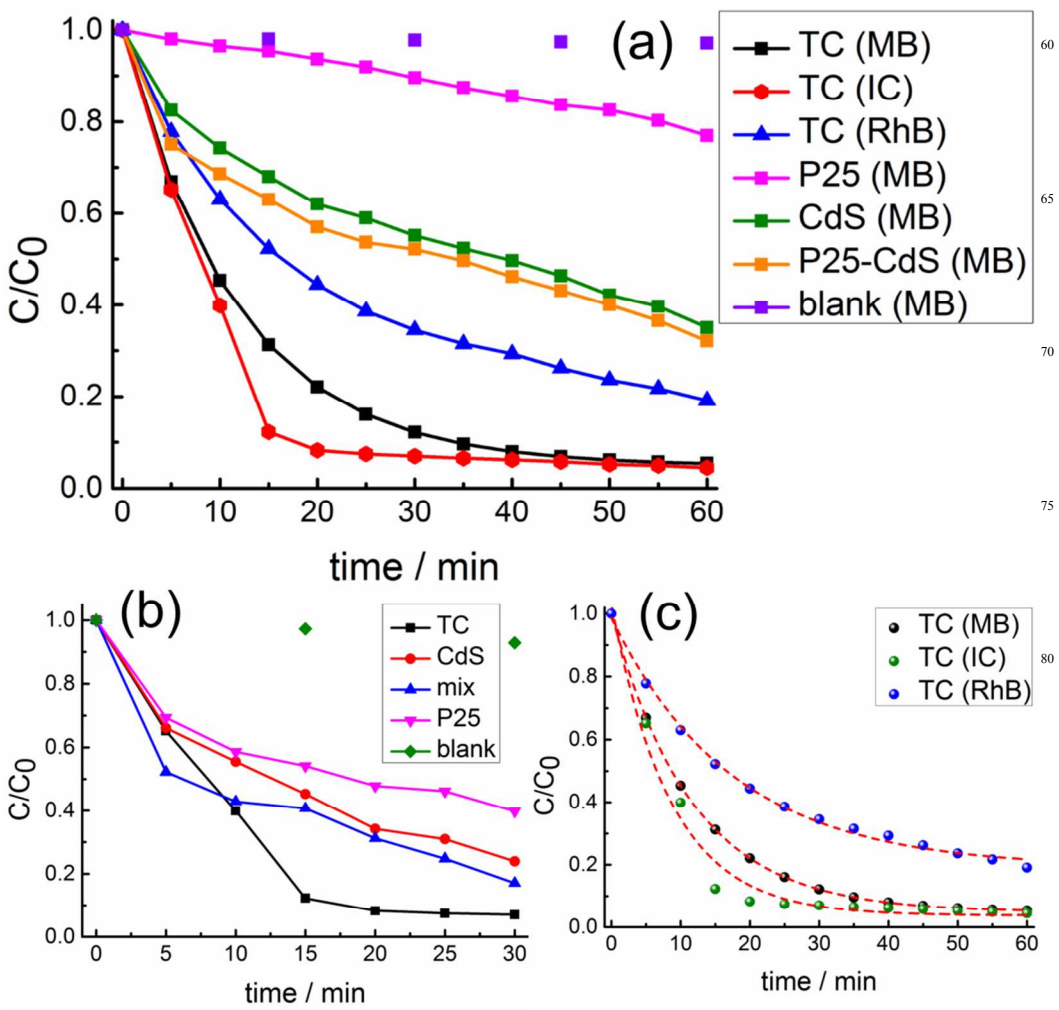

Figure 5. Dye-degradation profiles of the TiO_2-CdS microspheres (abbreviated as TC), commercial P25- TiO2, wurzite CdS and 1:1 physical mixture of wurzite CdS- P25- TiO2 also have been tested under similar conditions. Dyes mentioned in parenthesis are MB: methylene blue, IC: indigo carmine, RhB: rhodamine B. (a) MB dye degradation profile of all the samples along with the IC and RhB dye degradation by TC, (b) IC dye degradation profiles by all the samples and (c) first order exponential decay fittings for the sample TC for all the three dyes. Red dashed lines indicate the fits. Line joining points are a guide to eye in figures (a) and (b).

Cite this: DOI: 10.1039/c0xx00000x

www.rsc.org/xxxxxx

ARTICLE TYPE

Figure 5 shows the dye degradation profiles for TiO_2-CdS assembly, abbreviated hereafter as TC. Recently, Choi *et al* pointed out that the photocatalytic activity of a photocatalyst may be dye-specific and dye-degradation tests on multiple dyes rather than on a single one is prescribed to evaluate the intrinsic photocatalytic property of a material.[15] Based on this observation, photocatalytic activity of TC were performed on three separate dyes, namely methylene blue (MB) (a phenothiazine-cationic dye which is highly recommended due to its minimal absorption spectral overlap with the visible light photocatalyst and dye sensitization effect), indigo carmine (IC) (anionic dye) and rhodamine B (xanthene-Zwitter ionic dye). The absorption spectra were collected over a wide wavelength range (300 to 900 nm) using aliquots taken out at every 5 min intervals. This was done to monitor the formation of the degraded products rather than mere dye-mineralization. No other peaks other than that those related to the particular dye under investigation was observed. Figure 5 (a) depicts the degradation profiles of the MB dye due to TC and other samples. The degradation of IC and RhB by TC are also plotted in the same figure for comparison of the photocatalytic activity of TC. Figure 5 (b) shows only the degradation profiles of the dye IC. Sample TC is observed to be highly efficient and is able to degrade MB to one fifth of the starting concentration under 20 minutes. The degradation profile follows apparent first-order kinetics which is strongly evident from the one-exponential decay curve (figure 5 (c)). In comparison, the Degussa P25 exhibited very poor efficiency towards MB dye degradation. This is clearly due to poor light harvesting properties of the pristine TiO_2 under visible light. Due to wide band gap (= 3.2 eV), TiO_2 is predominantly activated under UV light which is only 4-5 % of the total light. [1b, 1c, 4] As a consequence, only a few electrons can be excited and the dye degradation is poor. The MB degradation by the wurtzite CdS sample is much slower than that of TC and it slightly improves when it's mixed with P25-TiO_2 (c/f table 1). TC is observed to be even more effective in degrading the IC dye, 90% of the dye solution degraded in 15 minutes. In case of degradation of IC as well, similar trends were observed with regard to the reference samples (wurtzite CdS and P25-TiO_2-CdS). Degradation of IC by CdS sample is less efficient than TC and improves marginally when mixed with P25-TiO_2. Figure 5 (a) and (b) also shows the degradation kinetics of the dyes in the absence of any semiconductor. On its own, the degradation of MB and IC dyes is negligible. This strongly suggests that the observed change in concentration as a function of time is not merely due to dye changes but rather to the degradation action induced by the TiO_2-CdS nano-heterostructure. The microspheres exhibit excellent reproducibility over few tens of cycles. This is evidenced from the photocatalytic efficiency obtained following several cycles (c/f figure S7). The nominal loss of photocatalytic activity over successive cycles may be attributed to the loss of the photocatalyst occurring during each round of retrieval, rinsing and transfer to the reaction vessel. The SEM images recorded as a function of the photocatalytic cycles showed similar profile after each cycle (c/f figure S7) and the elemental maps also suggested no change in the nano-heterostructure.

Table 1: Apparent first order rate constants of dye-degradation of various samples with different dyes.

sample	dye	k (min^{-1})
TC	Methylene Blue	0.085
CdS	MB	0.035
P25	MB	0.01
P25+CdS	MB	0.046
TC	Indigo Carmine	0.13
CdS	IC	0.071
P25	IC	0.022
P25+CdS	IC	0.078
TC	Rhodamine B	0.06

The recyclability of the P25-TiO_2:CdS sample was also monitored (c/f figure S8). However, a significant loss of photocatalytic activity is observed immediately after the first cycle due to photo-corrosion. Though photo-corrosion is a major concern of CdS photocatalysts, it can be eliminated by synthesizing optimized heterostructures where charge transfer from CdS to the other moiety can be easily facilitated. This leads to excellent stability and reusability.[2a] In our case, the tailored heterostructure prohibits any kind of corrosion of the photocatalyst as well as preserves the homogeneity even at nanometre length scale, thus facilitating efficient charge transfer from CdS to TiO_2 at various cycles. Hence, such semiconductor assemblies bear great promise for practical industrial applications. Apparent first order kinetics rate constant are estimated to be, k = 0.085 (± 0.001) min^{-1} for degradation of MB by the sample TC and k = 0.13 (± 0.016) min^{-1} for degradation of IC which are two order higher than the commercial TiO_2 (~ 0.001 min^{-1} for Degussa P25), almost double than that of the P25-CdS sample and several order higher compared to photocatalysis in absence of any semiconductor. The excellent degradation activity of TC can be attributed to better electron injection from the light harvester CdS to TiO_2. This result is also remarkable in the context of photocatalyst comprising of Au-tagged TiO_2. Though the rate constant is slightly higher [$k_{Au\text{-}TiO2}$ = 0.25 min^{-1}][7c] than that of TC, the slight inferior performance is offset by the cost effectiveness of the 'truly' one pot multi-gram synthesis from abundant materials employed here. The superior electron injection rate in case of TC is also strongly supported by the PL data which exhibits lesser emission than sample P25-CdS. As highlighted earlier, the interface characteristics here also plays an important role. The microporous nature of the sample and higher surface area also support it to gain an excellent photocatalytic activity under visible light.

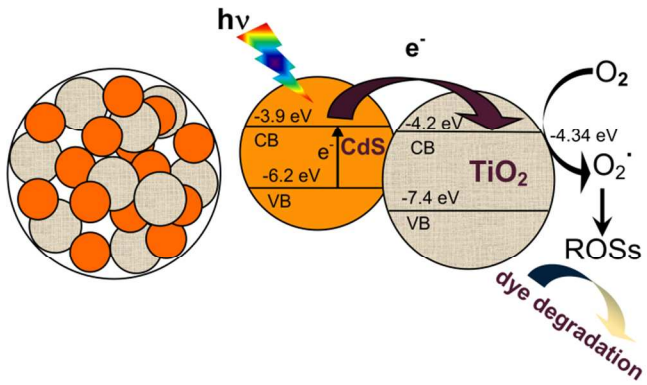

Scheme 1: Schematic depiction of dye degradation by nano-heterostructured TiO_2-CdS assembly under visible light. Reactive oxygen species is abbreviated as ROS. (E^0 O_2 (aq) /$O_2^{\bullet}$ = −4.34 eV). (pH ≈ 7).

Conclusions

The TiO_2-CdS microspheres have been convincingly demonstrated here as a potential visible light photocatalyst. The 'woollen knitting ball' like microspheres comprising of TiO_2 and CdS nanoparticles configured next to each other facilitate fast electron transfer rates which is evidenced by the ultra-high dye degradation rate constants compared to commercial products and other cost intensive noble metal based structures. We conclude that the combination of tailored micro- and nano- scale features result in very efficient photocatalysis under solar light. The semiconductors assembly discussed here will trigger manifold interests to synthesize various other semiconductor heterostructured assemblies for solar photon harvesting and related applications. The simplicity of usage of the photocatalyst, which can be achieved by merely placing it under the sun, has tremendous practical appeal especially in the realm of photo-degradation of industrial water pollutants.

Experimental Section

Materials and Methods

One pot synthesis of TiO_2-CdS heterostructured 'woollen knitting ball' like structure: The heterostructured materials were synthesized by a solvothermal method where titanium tetra isopropoxide (TTIP) was used as the Titania precursor and cadmium acetate and L-cysteine were used for synthesis of cadmium sulfide. The molar ratio used was TTIP: CTAB: HCl: H_2O: ethanol: $Cd(OAc)_2$: L-cysteine= 3.1: 1: 16: 167: 64: 1: 1. Cadmium acetate, L-cysteine and CTAB (surfactant) were taken in a dry Teflon container of 50 ml of capacity. De-ionized water and ethanol were added to it and it was kept in an ice-bath while stirring the mixture. After sufficient cooling TTIP and HCl were added drop wise one by one under vigorous stirring. After half an hour the container was taken out from the ice-bath but the stirring was continued inside a fume hood at room temperature (~ 30^0C) keeping the container uncapped to allow evaporation of the solvent with proper precaution to avoid any kind of contamination. After 6 h of stirring the volume of the aliquot was reduced to ~20 ml, then ~20 ml of DMF was added to it to make up the total volume ~40 ml under stirring. After few minutes of stirring the teflon container was capped and locked inside a stainless steel autoclave. Then, solvothermal reaction was carried out for 6 h at 150^0C. After proper cooling, the orange yellow product was collected by centrifugation and washed several times by milipore water and ethanol. It was dried at 70 ^{0}C in vacuum. The dried product was collected as powder and was subjected to further characterization and experiments.

Characterization: SEM images were taken by a Karl-Zeiss field-emitting scanning electron microscope under 5 kV of accelerating voltage. Lower voltage and small working distance was maintained to capture the surface features better of the micro spheres. EDS is also done using the same facility at higher accelerating voltage. Transmission Electron Microscopy and all other related experiments (HRTEM, SAED) were done using a JEOL-200kV FETEM. The TEM micrographs were studied by 'Digital Micrograph' software. The crystallographic phase identification of various materials was performed using powder X-ray diffraction (XRD; Philips X'Pert Pro diffractometer; Cu-Kα radiation, λ=1.5418 Å) with step width and scan rate of 0.02 and 2.50 per min respectively. Absorption spectra were recorded using a Lambda 35 UV-Vis spectrophotometer. Emission spectra were recorded by a Perkin Elmer Luminescence Spectrometer (LS-55). Solid samples were employed for both absorption and emission spectra.

Photocatalysis: 50 ml of 50 ppm dye solution was taken in a 100 ml beaker. To it 50 mg of as synthesized powder was added to maintain 1 g L^{-1} catalyst concentration. It was stirred in dark for 2 hours to reach the adsorption-desorption equilibrium. Then it was subjected to a vertical irradiation from a Oriel Class3A solar simulator (1 Sun, 1.5G AM). Aliquots were withdrawn in 5 min intervals. The aliquots were taken in a wrapped eppendorf to avoid further degradation due to exposure of light. It was centrifuged and the supernatant liquid was collected and subjected to absorbance spectroscopy by a UV-Vis spectrometer to measure the concentration of the undegraded dye from Lambert-Beer's law.

Acknowledgements

SM and AJB wishes to acknowledge CSIR, New Delhi, DST Nano Mission, New Delhi and India—Taiwan Programme of Cooperation in Science & Technology Project towards financial support of the work. The authors also acknowledge Prof. S. Natarajan, SSCU, IISc. Bangalore, AFMM IISc. Bangalore and CENSE, IISc. Bangalore for instrument support and Ms. N. Jain for useful discussions.

Notes and references

a Solid State and Structural Chemistry Unit, Indian Institute of Science, Bangalore-560012, INDIA
E-mail: aninda_jb@sscu.iisc.ernet.in;
FAX: +91 8023601310

†Electronic Supplementary Information (ESI) available: More SEM and HRTEM images, BET, BJH, N_2 adsorption/desorption isotherm, XPS, recyclibility of the TiO_2-CdS microsphere assembly and the benchmark sample as a photocatalyst.

See DOI: 10.1039/b000000x/

1. a) T. S. Teets and D. G. Nocera, *Chem. Commun.,* 2011, **47,** 9268.; b) M. R. Hoffmann, S. T. Martin, W. Y. Choi and D. W. Bahnemann, *Chem. Rev.,* 1995, **95,** 69.; c) I. K. Konstantinou and T. A. Albanis, *Appl. Catal., B,* 2004, **49,** 1.; d) S. Dong, J. Feng, M. Fan, Y. Pi, L. Hu, X. Han, M. Liu, J. Sun and J. Sun, *RSC Adv.*, 2015, **5**, 14610.; e) X. Wang, Y. Ying, J. Lei, P. Hu and X. Peng, *RSC Adv.*, 2014, **4**, 42441.; f) Y.-S. Hu, Y.-G. Guo, W. Sigle, S. Hore, P. Balaya and J. Maier, *Nat. Mater.,* 2006, **5**, 713.; g) A. Perro, S. Reculusa, F. Pereira, M. H. Delville, C. Mingotaud, E. Duguet, E. Bourgeat-Lami and S. Ravaine, *Chem. Commun.,* 2005, 5542.; h) P. V. Kamat, *J. Phys. Chem. C,* 2008, **112,** 18737.

2. a) Y. Min, G. He, Q. Xu and Y. Chen, *J. Mater. Chem A*. **2014,** *2,* 2578.; b) P. Garrigue, M. H. Delville, C. Labrugere, E. Cloutet, P. J. Kulesza, J. P. Morand and A. Kuhn, *Chem. Mater.,* 2004, **16,** 2984.; c) S. R. Gajjela, K. Ananthanarayanan, C. Yap, M. Graetzel and P. Balaya, *Energy Environ. Sci.,* 2010, **3,** 838.; d) T. Tachikawa, S. Yamashita and T. Majima, *Angew. Chem. Int. Ed.,* 2010, **49,** 432.; e) X. Yu, A. Shavel, X. An, Z. Luo, M. Ibáñez and A. Cabot, *J. Am. Chem. Soc.,* 2014, **136,** 9236.; f) X. Yu, X. An, A. Shavel, M. Ibanez and A. Cabot, *J. Mater. Chem. A,* 2014, **2,** 12317. g) Z. Xiong and X. S. Zhao, *RSC Adv.*, 2014, **4**, 61960.; h) S. S. Qian, C. S. Wang, W. J. Liu, Y. H. Zhu, W. J. Yao, X. H. Lu, *J. Mater. Chem*. **2011,** *21,* 4945.; i) K. Zhao, Z. Wu, R. Tang, Y. Jiang and Y. Lu, *Res Chem Intermed*, 2014, 1.; j) X. Li, J. Yu, J. Low, Y. Fang, J. Xiao and X. Chen, *J. Mater. Chem. A*, 2015, **3,** 2485.; k) H. Wang, L. Zhang, Z. Chen, J. Hu, S. Li, Z. Wang, J. Liu and X. Wang, *Chem. Soc. Rev.* 2014, **43,** 5234.; l) Y.-P. Yuan, L.-W. Ruan, J. Barber, S.C. Joachim Loo, C. Xue, *Energy Environ. Sci.*, 2014, **7,** 3934.

3. a) H. B. Wu, H. H. Hng and X. W. Lou, *Adv. Mater.,* 2012, **24,** 2567.; b) S. R. Gajjela, C. Yap and P. Balaya, *J. Mater. Chem.,* 2012, **22**, 10873.; c) Z. Tebby, O. Babot, T. Toupance, D.-H. Park, G. Campet and M.-H. Delville, *Chem. Mater.,* 2008, **20,** 7260.; d) S. Sarkar, R. Das, H. Choi and C. Bhattacharjee, *RSC Adv.*, 2014, **4**, 57250.; e) A. Ajmal, I. Majeed, R. N. Malik, H. Idriss and M. A. Nadeem, *RSC Adv.*, 2014, 4, 37003.

4. a) Q. Sun and Y. Xu, J. Phys. Chem. C, 2009, **113,** 12387.; b) H. Zhang, X. Lv, Y. Li, Y. Wang and J. Li, *ACS Nano,* 2009, **4,** 380.

5. a) W. Qin, D. Zhang, D. Zhao, L. Wang and K. Zheng, *Chem. Commun.,* 2010, **46,** 2304.; b) C. Fabrega, T. Andreu, A. Cabot and J. R. Morante, *J. Photochem. Photobiol. A-Chem.,* 2010, **211,** 170.

6. a) S. Pany, K. M. Parida and B. Naik, *RSC Adv.*, 2013, **3**, 4976.; b) W. Kim, T. Tachikawa, H. Kim, N. Lakshminarasimhan, P. Murugan, H. Park, T. Majima and W. Choi, *Appl. Catal., B,* 2014, **147,** 642.

7. a) S. S. Mandal and A. J. Bhattacharyya, *J. Chem. Sci.,* 2012, **124,** 969.; b) R. Nafria, P. R. de la Piscina, N. Homs, J. R. Morante, A. Cabot, U. Diaz and A. Corma, *J. Mater. Chem. A,* 2013, **1,** 14170.; c) Z. Bian, T. Tachikawa, P. Zhang, M. Fujitsuka and T. Majima, *J. Am. Chem. Soc.,* 2013, **136,** 458.

8. a) B. Ayoubi-Feiz, S. Aber and M. Sheydaei, *RSC Adv.*, 2015, **5**, 19368.; b) K. H. Wong, K. Ananthanarayanan, S. R. Gajjela and P. , Balaya, *Mater. Chem. Phys.,* 2011, **125,** 553.

9. a) E. Elmalem, A. E. Saunders, R. Costi, A. Salant and U. Banin, *Adv. Mater.,* 2008, **20,** 4312.; b) G. Manna, R. Bose and N. Pradhan, *Angew. Chem. Int. Ed.,* 2014, **53,** 6743.; c) T. Yan, H. Zhang, Y. Liu, W. Guan, J. Long, W. Li and J. You, *RSC Adv.*, 2014, **4**, 37220.

10. a) Z. Wang, J. Hou, C. Yang, S. Jiao and H. Zhu, *Chem. Commun.,* 2014, **50,** 1731.; b) B. Liu, L.-M. Liu, X.-F. Lang, H.-Y. Wang, X. W. Lou and E. S. Aydil, *Energy Environ. Sci.,* 2014, **7,** 2592.; c) S. Mazumdar and A. J. Bhattacharyya, *Energy Environ. Sci.,* 2013, **6,** 1494.; d) A. Salant, M. Shalom, I. Hod, A. Faust, A. Zaban and U. Banin, *ACS Nano,* 2010, **4,** 5962. ; e) X. Li, T. Xia, C. Xu, J. Murowchick and X. Chen, *Catal. Today.*, 2014, **225,** 64.; f) L. Qi, J. Yu and M. Jaroniec, *Phys. Chem. Chem. Phys.*, 2011, **13,** 8915.; g) G.-S. Li, D.-Q. Zhang and J. C. Yu, *Environ. Sci. Technol.*, 2009, **43,** 7079.; h) Z. Chen and Y.-J. Xu, *Acs Appl. Mater. Inter.*, 2013, **5,** 13353.

11. a) Y. Hu, X. Gao, L. Yu, Y. Wang, J. Ning, S. Xu and X. W. Lou, *Angew. Chem. Int. Ed.,* 2013, **52,** 5636. b) J. Yuan, J. Wen, Q. Gao, S. Chen, J. Li, X. Li and Y. Fang, *Dalton Trans.*, 2015, **44,** 1680.; c) X. Li, J. Chen, H. Li, J. Li, Y. Xu, Y. Liu and J. Zhou, *J. Nat. Gas. Chem.*, 2011, **20,** 413.; d) J. Yu, Y. Yu, P. Zhou, W. Xiao and B. Cheng, *Appl. Catal. B-Environ.*, 2014, **156–157**, 184.; e) J. Zhang, S. Z. Qiao, L. Qi and J. Yu, *Phys. Chem. Chem. Phys.*, 2013, **15,** 12088.; f) Q. Xiang, B. Cheng and J. Yu, *Appl. Catal. B-Environ.*, 2013, **138,** 299.

12. a) P. V. Kamat, *Acc. Chem. Res.,* 2012, **45,** 1906.; b) P. V. Kamat, K. Tvrdy, D. R. Baker and J. G. Radich, *Chem. Rev.,* 2010, **110,** 6664.; c) A. J. Nozik and R. Memming, *J. Phys. Chem.,* 1996, **100,** 13061.

13. H. Chu, X. Li, G. Chen, W. Zhou, Y. Zhang, Z. Jin, J. Xu and Y. Li, *Cryst. Growth Des.,* 2005, **5,** 1801.

14. I. Robel, M. Kuno and P. V. Kamat, *J. Am. Chem. Soc.,* 2007, **129,** 4136.

15. S. Bae, S. Kim, S. Lee and W. Choi, *Catal. Today.*, **2014**, *224*, 21.